6184–6197 *Nucleic Acids Research, 2020, Vol. 48, No. 11* *Published online 6 May 2020*
doi: 10.1093/nar/gkaa301

DIS3L2 and LSm proteins are involved in the surveillance of Sm ring-deficient snRNAs

Adriana Roithová[1,2], Zuzana Feketová[3], Štěpánka Vaňáčová[3] and David Staněk[1,*]

[1]Laboratory of RNA Biology, Institute of Molecular Genetics of the Czech Academy of Sciences, Videnska 1083, 14220 Prague, Czech Republic, [2]Faculty of Science, Charles University, 128 00 Prague, Czech Republic and [3]CEITEC—Central European Institute of Technology, Masaryk University, Kamenice 5/A35, 625 00 Brno, Czech Republic

Received December 19, 2019; Revised April 6, 2020; Editorial Decision April 16, 2020; Accepted April 23, 2020

ABSTRACT

Spliceosomal small nuclear ribonucleoprotein particles (snRNPs) undergo a complex maturation pathway containing multiple steps in the nucleus and in the cytoplasm. snRNP biogenesis is strictly proofread and several quality control checkpoints are placed along the pathway. Here, we analyzed the fate of small nuclear RNAs (snRNAs) that are unable to acquire a ring of Sm proteins. We showed that snRNAs lacking the Sm ring are unstable and accumulate in P-bodies in an LSm1-dependent manner. We further provide evidence that defective snRNAs without the Sm binding site are uridylated at the 3′ end and associate with DIS3L2 3′→5′ exoribonuclease and LSm proteins. Finally, inhibition of 5′→3′ exoribonuclease XRN1 increases association of ΔSm snRNAs with DIS3L2, which indicates competition and compensation between these two degradation enzymes. Together, we provide evidence that defective snRNAs without the Sm ring are uridylated and degraded by alternative pathways involving either DIS3L2 or LSm proteins and XRN1.

INTRODUCTION

Spliceosomal small nuclear RNAs (snRNAs) are essential components of the spliceosome and three of them—U2, U5 and U6—form the catalytic center of this complex. snRNAs enter the splicing reaction associated with proteins in complexes called small nuclear ribonucleoprotein particles (snRNPs). Before snRNPs join the spliceosome, they undergo a complex maturation pathway that involves several chaperon complexes, including PRMT5, SMN and R2TP/HSP90 [reviewed in (1–4)]. All spliceosomal snRNAs transcribed by RNA polymerase II are after their synthesis exported to the cytoplasm, where they are bound by Gemin5 of the SMN complex (5–7). The SMN complex together with the PRMT5 complex promotes assembly of a heptameric Sm ring around the Sm binding site (8–11). Following the Sm ring formation, the monomethyl 5′ cap is trimethylated and the 3′ end is trimmed. Both the Sm ring and the trimethyl cap are key signals for reimport of a newly formed core snRNP back into the nucleus [reviewed in (12)]. In the cell nucleus, newly imported snRNPs first appear in Cajal bodies, where snRNAs are post-transcriptionally modified and snRNP biogenesis is finalized by addition of snRNP-specific proteins (13,14). snRNP-specific proteins are folded and pre-assembled in the cytoplasm by SMN and R2TP/HSP90 chaperon complexes and imported into the nucleus independently of core snRNPs (15–17). The mature snRNPs leave the Cajal body and participate in pre-mRNA splicing (18).

Along the snRNP biogenesis pathway, there are several quality control checkpoints that safeguard the formation of key assembly intermediates. Newly transcribed pre-snRNAs are in the nucleus processed at their 3′ end by the integrator complex (19). Several studies have reported that misprocessed pre-snRNAs are oligouridylated [oligo(U)] at the 3′ end and subsequently targeted by oligo(U)-specific exoribonuclease DIS3L2 (20–22). New pre-snRNAs interact with coilin and accumulate in Cajal bodies, where they are retained until the export complex is formed (23–25). After export to the cytoplasm, pre-snRNAs associate with the SMN complex that orchestrates the cytoplasmic phase and Sm ring formation (4,9,26). Sm proteins themselves are tightly regulated by controlled association with ribosomes and the PRMT5 complex (2,27,28). The Sm ring targets core snRNPs back to the nucleus and to Cajal bodies, where core snRNPs are sequestered until their final maturation (18,29–31). Inhibition of the Sm ring assembly leads to destabilization of Sm proteins and snRNAs in somatic cells (27,32,33). Truncated snRNA transcripts that fail to acquire the Sm ring are localized to cytoplasmic P-bodies. There are two major exoribonucleolytic activities in the cytoplasm of mammalian cells: the 5′→3′ exonuclease XRN1 and the 3′→5′ trimming catalyzed by the RNA exosome (34). However, oligo(U) tailed RNAs are primarily targeted by 3′→5′ exoribonuclease DIS3L2 and in some spe-

*To whom correspondence should be addressed. Tel: +420 2 96443118; Fax: +420 224 310 955; Email: stanek@img.cas.cz

© The Author(s) 2020. Published by Oxford University Press on behalf of Nucleic Acids Research.
This is an Open Access article distributed under the terms of the Creative Commons Attribution Non-Commercial License (http://creativecommons.org/licenses/by-nc/4.0/), which permits non-commercial re-use, distribution, and reproduction in any medium, provided the original work is properly cited. For commercial re-use, please contact journals.permissions@oup.com

cific coding and noncoding RNAs also by ERI1 and USB1 (35,36). Previous studies proposed that truncated snRNA transcripts are primarily degraded by the 5′→3′ exonuclease XRN1 because downregulation of the 3′ to 5′ decay factors such as DIS3L2 and exosome did not lead to stabilization of truncated U1 and U2 snRNA transcripts lacking the Sm binding site (32,33,37). The XRN1-mediated decay depends on additional reactions, such as the 5′ cap removal by DCP2 that functions in a complex with DCP1 (38–40). The DCP2 activity is further enhanced by the conserved Pat1/LSm1–7 complex (41–44). The Lsm1–7 proteins form a ring that interacts with 3′ oligouridylated or oligoadenylated RNAs *in vivo* and displays higher affinity to oligo(U) *in vitro* (35,45–49).

One of the key questions remaining is how cells distinguish between functional and defective snRNA/snRNP. The Cajal body targeting and accumulation of incomplete snRNPs depends on splicing factor SART3 and Sm proteins (18,31). In the cytoplasm, Gemin5 was suggested to be the factor that recognizes U1 snRNA lacking the Sm site and sequesters them in P-bodies (7,50). In this study, we use microinjection of fluorescently labeled snRNAs, expression of MS2-tagged snRNAs and *in situ* detection of endogenous snRNAs to monitor localization of snRNAs lacking the Sm binding site and/or the Sm ring and to identify proteins that interact with these defective snRNAs. We combined these approaches with knockdown and knockout of proteins implicated in the cytoplasmic RNA decay and determined factors important for P-body accumulation and degradation of U1 and U2 snRNAs without the Sm ring.

MATERIALS AND METHODS

Cell culture

T-REx-HeLa (Invitrogen) DIS3L2^{KO} and DIS3L2$^{KO+D391N}$ cell lines were prepared as described previously (20,51). See Supplementary Figure S1 for induced expression of DIS3L2^{D391N} in the DIS3L2$^{KO+D391N}$ cell line. T-REx-HeLa and HEK DIS3L2^{KO} and DIS3L2$^{KO+D391N}$ cell lines (20,51) were cultured in Dulbecco's modified Eagle's medium containing 4.5 g glucose/l (Sigma) supplemented with 10% fetal bovine serum (FBS), 1% penicillin and streptomycin (Gibco). The T-REx-HeLa DIS3L2$^{KO+D391N}$ and HEK DIS3L2$^{KO+D391N}$ cell lines was supplemented with 10% FBS tetracycline-free (Biosera) and 1% penicillin and streptomycin (Gibco).

Plasmids

The U2 snRNA-MS2 construct, which includes the promoter sequence (bp 563 nt upstream of U2 transcription start site), was prepared from HeLa genomic DNA as described earlier (31). Deletion of the Sm site (U2ΔSm-MS2) was performed by site-directed mutagenesis using primers DelU2Sm-F and DelU2Sm-R (see Supplementary Table S1). Insertion of the XRN1-resistant sequence (GGGCGTAACCTCCATCCGAGTTGCAAGAGAGG AAACGCAGTCTC) to the 5′ end of the U2 snRNA to create U2wt_xrRNA-MS2 and U2ΔSm_xrRNA-MS2 was done by site-directed mutagenesis using primers xrRNA-F and xrRNA-R (see Supplementary Table S1).

The U1 snRNA construct, which contains an endogenous promoter and the U1 snRNA sequence, was kindly provided by F. Pagani (ICGEB, Trieste, Italy). The MS2 loop was inserted into stem loop IV by site-directed mutagenesis using primers U1-MS2-F and U1-MS2-R (see Supplementary Table S1). The U1 snRNA-MS2 construct lacking the Sm site (U1ΔSm-MS2) was created by site-directed mutagenesis using primers DelU1Sm-F and DelU1Sm-R (see Supplementary Table S1). Lsm1 was cloned from total HeLa RNA by reverse transcription (RT) followed by polymerase chain reaction (PCR) using specific primers Lsm1-F and Lsm1-R (see Supplementary Table S1) and cloned into the GFP-N2 vector (Clontech) using EcoRI/BamHI restriction sites.

Antibodies

For indirect immunostaining, we used anti-coilin (5P10) antibody, kindly provided by M. Carmo-Fonseca (Institute of Molecular Medicine, Lisboa), anti-DDX6 antibody (Promega), anti-Gemin2 antibody (Santa Cruz), anti-SMN 2B1 antibody (Santa Cruz) and anti-Gemin5 antibody (Millipore). Secondary anti-mouse antibodies conjugated with Alexa-647 and Alexa-405 (Invitrogen) were used. For immunoprecipitation, we used anti-goat GFP antibodies kindly provided by Pavel Tomancak (MPI-CBG Dresden, Germany) and mouse anti-FLAG M2 (Sigma). For western blotting, we used mouse anti-GFP (Santa Cruz), mouse anti-XRN1 (C-1; Santa Cruz), mouse anti-DCP2 (Santa Cruz) and anti-DIS3L2 (51). Secondary goat anti-mouse or anti-rabbit antibodies conjugated with horseradish peroxidase (Jackson ImmunoResearch Laboratories) were used.

RNAi

siRNAs used in this study were XRN1 (5′-GAGAGUAUAUUGACUAUGAtt-3′, 20 nM, Thermo Fisher), SmB/B′ (5′-UCUACUGUCAUUGAGACCAga-3′, 20 nM, Thermo Fisher), DCP2 (5′-CUUGCUCG UUUGUACAUCAtt-3′, 20 nM, Thermo Fisher), Lsm1 (5′-GAAGGACACUUAUAGGCUUtt-3′, 20 nM, Thermo Fisher) and esiRNA SMN1 (5′-CCAGAGCGATGATTCTGACATTTGGGATGA TACAGCACTGATAAAAGCATATGATAA, 20 nM, Sigma-Aldrich). siRNAs were transfected with Oligofectamine (Invitrogen) according to the manufacturer's protocol. Cells were microinjected or fixed 48 h (siRNAs SmB/B′, DCP2, Lsm1) or 72 h (siRNAs SMN, XRN1) after transfection. The 'negative control 5' siRNA from Invitrogen was used as a negative control. Control western blots that document RNAi-induced protein degradation are presented in Supplementary Figure S2.

In vitro transcription

All DNA templates for *in vitro* transcription were prepared by PCR using Phusion polymerase (Biolab) and plasmids containing either full-length snRNA or snRNA lacking the Sm site (ΔSm) as templates as described previously (31). The template of the U2ΔSmΔSMN mutant was created by PCR using Phusion polymerase (Biolab) with specific

primers T7-U2-F and U2ΔSm-R (see Supplementary Table S1). Fluorescently labeled RNAs were prepared as described previously (31) by *in vitro* transcription using a Megashortscript III kit (Thermo Fisher) containing UTP-Alexa-488 (Thermo Fisher) and trimethylated cap analog ($m_3^{2,2,7}$G(5′)ppp(5′)G) (Jena Bioscience) or monomethyl cap analog (m^7G(5′)ppp(5′)G) (Thermo Fisher). After synthesis, RNA was isolated by phenol/chloroform extraction, precipitated and dissolved in nuclease-free water. RNA was diluted in a solution containing Dextran-TRITC 70 kDa (Sigma-Aldrich) to the final concentration of 200 ng/μl.

Microinjection

HeLa cells were grown on glass coverslips for 24 h and RNA was microinjected using InjectMan 2 coupled with FemtoJet (Eppendorf) as described previously (31) using injection pressure (P_i) of 170 hPa and compensation pressure (P_c) of 50 hPa. The cells were incubated for 60 min at 37°C and then fixed. TRITC-Dextran (MW 70 kDa; Sigma) was used at a final concentration of 10 μg/μl from a stock solution (40 μg/μl) and mixed with the injected snRNA as a marker.

Indirect immunofluorescence and image acquisition

HeLa cells grown on coverslips were washed with phosphate-buffered saline (PBS) and fixed with 4% (w/v) paraformaldehyde in piperazine-*N*,*N*′-bis(2-ethanesulfonic acid) (PIPES) for 20 min at room temperature. Cells were permeabilized with 0.5% Triton X-100 (Sigma-Aldrich) in PBS for 5 min at room temperature and blocked with 5% goat serum in PBS (Jackson ImmunoResearch) for 10 min at room temperature. The cells were then incubated with primary and secondary antibodies for 1 h each at room temperature. Images were acquired using the DeltaVision microscopic system (Applied Precision) coupled to an Olympus IX70 microscope equipped with an oil immersion 63× objective/1.42 NA Photometrics CoolSNAP HQ2 camera (Princeton Instruments) and acquisition software SoftWorx (Applied Precision). Stacks of 20 z-sections with 200 nm z-steps were collected per sample and subjected to mathematical deconvolution using SoftWorx software. Maximal projections of deconvolved pictures were generated by SoftWorx and are presented.

snRNP precipitation

Immunoprecipitation was performed as previously described (52) using goat anti-GFP antibodies 24 h after transfection of MS2-snRNAs + MS2-YFP or Lsm1-GFP (31). Briefly, cells were washed in PBS, scrapped into a tube and resuspended in NET-2 buffer (50 mM Tris–HCl, pH 7.5, 150 mM NaCl, 0.05% Nonidet P-40) supplemented with protease inhibitor cocktail (Calbiochem) and pulse sonicated on ice (3 × 30 pulses, each pulse 0.5 s at 40% of maximum energy). The cell lysate was centrifuged at 20 000 × *g* and the supernatant was immunoprecipitated overnight at 4°C with 7.5 μg of goat anti-GFP antibodies pre-bound to 20 μl of Protein-G Agarose beads (Santa Cruz). RNA was extracted using phenol/chloroform, resolved in polyacrylamide gel containing 7 M urea and stained with silver. The immunoprecipitated proteins were resuspended in 30 μl of 2× sample buffer (0.25 M Tris–HCl, pH 6.8, 20% glycerol, 4% sodium dodecyl sulfate, 2% β-mercaptoethanol, 0.02% bromphenol blue), resolved in 12% polyacrylamide gel and detected by western blotting.

3′ RACE-based detection of the uridylation status of snRNA 3′ ends

T-REx-HeLa control cell line and DIS3L2$^{KO+D391N}$ cell line were grown to 50% confluence. The cells were transfected with 20 nM control or Xrn1 siRNAs using Lipofectamine RNAiMAX (Invitrogen) according to the manufacturer's protocol. After 48 h incubation at 37°C, the cells were transfected with one of the plasmids expressing different forms of U1 and U2 snRNAs (U1wt-MS2, U1ΔSm-MS2, U2wt-MS2 and U2ΔSm-MS2) using Turbofect (Thermo Scientific) according to the manufacturer's protocol. The DIS3L2 expression was induced with doxycycline (100 ng/ml) 16 h prior to harvesting (56 h after the first siRNA treatment). Cells were harvested and the small RNA fraction was isolated using TriPure Isolation Reagent (Roche) followed by selective RNA precipitation as described previously (20). Purified RNA was treated with Turbo DNase (Ambion) followed by phenol/chloroform extraction and isopropanol precipitation. Small RNA (1.7 μg) was incubated with 2 μl of 10 μM of the L3AppDNA 3′ terminal linker (5rApp/AGATCGGAAGAGCACACGTCT/3ddC, IDT) and 200 U of the T4 RNA Ligase2, truncated K227Q (New England BioLabs) in 20 μl of total reaction volume at 16°C overnight. RNA was reverse-transcribed with SuperScript III (Invitrogen) using RT-CLIP2 primer. Equal amounts of RNA were used for the linker ligation step and master mixes were used when comparing different cell lines and samples. PCR was typically performed with linker-specific reverse and forward gene-specific primers. The PCR products were isolated from the gel, cloned into pDRIVE (Qiagen) and analyzed by Sanger sequencing.

RNA immunoprecipitation

Cells grown to 80% confluence were washed with ice-cold PBS and UV cross-linked (2 × 200 mJ of 254 nm UV). Cells were collected, frozen in liquid nitrogen and stored at −80°C. Pellets were placed on ice and lysed in lysis buffer [LB, containing 50 mM Tris, pH 7.5, 0.5% Triton X-100, 150 mM NaCl, supplemented with 1 mM dithiothreitol, protease inhibitor cocktail (Roche) and RNase inhibitor RNAsin (Promega)] and the insoluble fraction was sedimented by centrifugation. FLAG-tagged DIS3L2^{D391N} was immunoprecipitated using anti-FLAG M2 Magnetic Beads (Sigma). Bound protein–RNA complexes were extensively washed with LB containing 300 mM NaCl and treated with Turbo DNase (Ambion). Material was released from the beads by incubation with 4 U of Proteinase K (NEB) for 1 h at 37°C and again with 4 U for 1 h at 45°C. RNA was purified using phenol/chloroform extraction and precipitated with isopropanol. The same RNA amount from all samples was used for further processing. Enzymes and chemicals were scaled according to the RNA amount for each ex-

periment. 3′ Linker ligation and reverse transcription were performed as mentioned earlier.

RT-qPCR analysis

RNA was isolated from immunoprecipitation by phenol/chloroform extraction and analyzed by RT-qPCR. RT was performed using SuperScript III RT (Invitrogen) and random hexamers (Eastport). The synthesis was performed as follows: 5 min at 65°C, 5 min at 25°C and 1 h at 50°C. The inactivation was 15 min at 75°C. The cDNA was analyzed by qPCR using a Roche Light Cycler 480 standard protocol (45 cycles, 60°C annealing). To detect U1-MS2 and U2-MS2 snRNAs, MS2-rev primer was used for RT and U1WT-F and U2WT-F and MS2-rev for PCR. The primers used to amplify individual snRNAs are listed in Supplementary Table S1.

Fluorescence *in situ* hybridization

Cy3-labeled DNA probes were used against U1, U2 and U4 snRNAs as previously described (18):

U1 snRNA: 5′Cy3-CCTTCGTGATCATGGTATCTCC CCTGCCAGGTAAGTAT-3′
U2 snRNA: 5′Cy3-GAACAGATACTACACTTGATCT TAGCCAAAAGGCCGAGAAGC-3′
U4 snRNA: 5′Cy3-TCACGGCGGGGTATTGGGAAAA GTTTTCAATTAGCAATAATCGCGCCT-3′

Forty-eight to seventy-two hours after siRNA transfection, cells were fixed in 4% paraformaldehyde/PIPES (Sigma) for 15 min, permeabilized with 0.5% Triton X-100 for 5 min and incubated with anti-DDX6 antibodies as a marker of P-bodies followed by incubation with secondary antibody conjugated with Alexa-647 (Life Technologies). Cells were again fixed in 4% paraformaldehyde/PIPES for 5 min, quenched for 5 min in 0.1 M glycine/0.2 M Tris, pH 7.4, and incubated with Cy3-labeled probes in 2× SSC/50% formamide/10% dextran sulfate/1% bovine serum albumin for 60 min at 37°C. After washing in 2× SSC/50% formamide, 2× SSC and 1× SSC, coverslips were mounted to microscope slides using Fluoromount G containing 4′,6-diamidino-2-phenylindole (DAPI) (Southern Biotech) for DNA staining. Images were collected using a DeltaVision microscope system as described earlier.

RESULTS

snRNAs lacking the Sm ring localize into P-bodies

We used three independent approaches to monitor the subcellular localization of snRNAs with or without the Sm ring. First, we prepared expression vectors containing natural U1 or U2 snRNA promoters followed by U1 or U2 snRNA natural sequences. We inserted an MS2 binding site into the stem loop IV of U1 snRNA and into the stem loop IIb of U2 snRNA (Figure 1A). We have previously shown that the U2-MS2 snRNA correctly assembled with Sm proteins and U2-specific proteins *in vivo* (31). To test whether the U1-MS2 snRNA binds Sm proteins and U1-specific proteins, we co-transfected U1-MS2 snRNA with an expression plasmid encoding MS2 protein tagged with YFP (MS2-YFP) and immunopurified MS2-YFP-bound U1-MS2 snRNPs by anti-GFP antibodies that cross-react with the YFP protein. Although we cannot prove that MS2-containing snRNAs are splicing competent, western blot analysis of co-precipitated proteins showed that the insertion of the MS2 binding site did not inhibit binding of Sm proteins and U1-specific proteins U1A and U1-70K to U1-MS2 snRNA (Supplementary Figure S3). To test the effect of Sm site deletion on MS2-tagged snRNA localization, we removed the Sm binding site from U1-MS2 and U2-MS2 snRNAs (U1ΔSm-MS2 and U2ΔSm-MS2) and co-expressed them with the MS2-YFP protein (Figure 1A). Whereas the wild-type (WT) snRNAs accumulated in nuclear Cajal bodies, snRNAs lacking the Sm site accumulated in the cytoplasm, where they co-localized with P-body marker DDX6 (Figure 1B).

A second approach was based on microinjection of fluorescently labeled snRNAs into the cytoplasm of human cells. snRNAs, either full length or without the Sm site, were *in vitro* transcribed in the presence of Alexa-488-UTP that allows for direct detection by fluorescence microscopy. After purification, snRNAs were microinjected into the cytoplasm of HeLa cells together with Dextran-70kDa-TRITC to monitor the injection site. After 1 h incubation, the cells were fixed and localization of microinjected snRNAs was detected by fluorescence microscopy. Both WT U1 and U2 snRNAs were transported to the nucleus, where they accumulated in Cajal bodies as previously described (31). Consistently with the localization of ΔSm-MS2 snRNAs, microinjected snRNAs lacking the Sm site remained in the cytoplasm and accumulated in P-bodies (Figure 1C).

Finally, we prevented formation of the complete Sm ring by RNAi-mediated knockdown of the SmB/B′ protein, an essential component of the Sm ring. A subcore snRNP lacking SmB/B′ and D3 proteins has been described *in vitro* (8), but whether it is able to stabilize snRNAs *in vivo* is currently unclear. We monitored the localization of endogenous snRNAs by *in situ* hybridization and revealed a P-body accumulation of endogenous snRNAs upon SmB/B′ knockdown (Figure 2A). This result is consistent with our previous data and suggests that if the subcore snRNP without SmB/B′ is formed, it is not able to prevent snRNA accumulation in P-bodies. It should be noted that the P-body accumulation of snRNAs after depletion of SmB/B′ was not observed in all cells. Surprisingly, not all P-bodies within a single cell contained the snRNA signal. However, those P-bodies that accumulated snRNAs also showed a signal for SMN complex components—the SMN protein, Gemin2 and Gemin5 (Figure 2B and Supplementary Figure S4). The SMN protein is a scaffolding protein of the SMN complex. To test whether the SMN protein is important for accumulation of Gemin2 and Gemin5 in snRNA-positive P-bodies, we knocked down SmB/B′ together with the SMN protein and monitored the P-body localization of endogenous U2 snRNA together with Gemin2 and Gemin5 (Supplementary Figure S4). Our data show that Gemin2 and Gemin5 co-localize with U2 snRNA in P-bodies independently of the SMN protein.

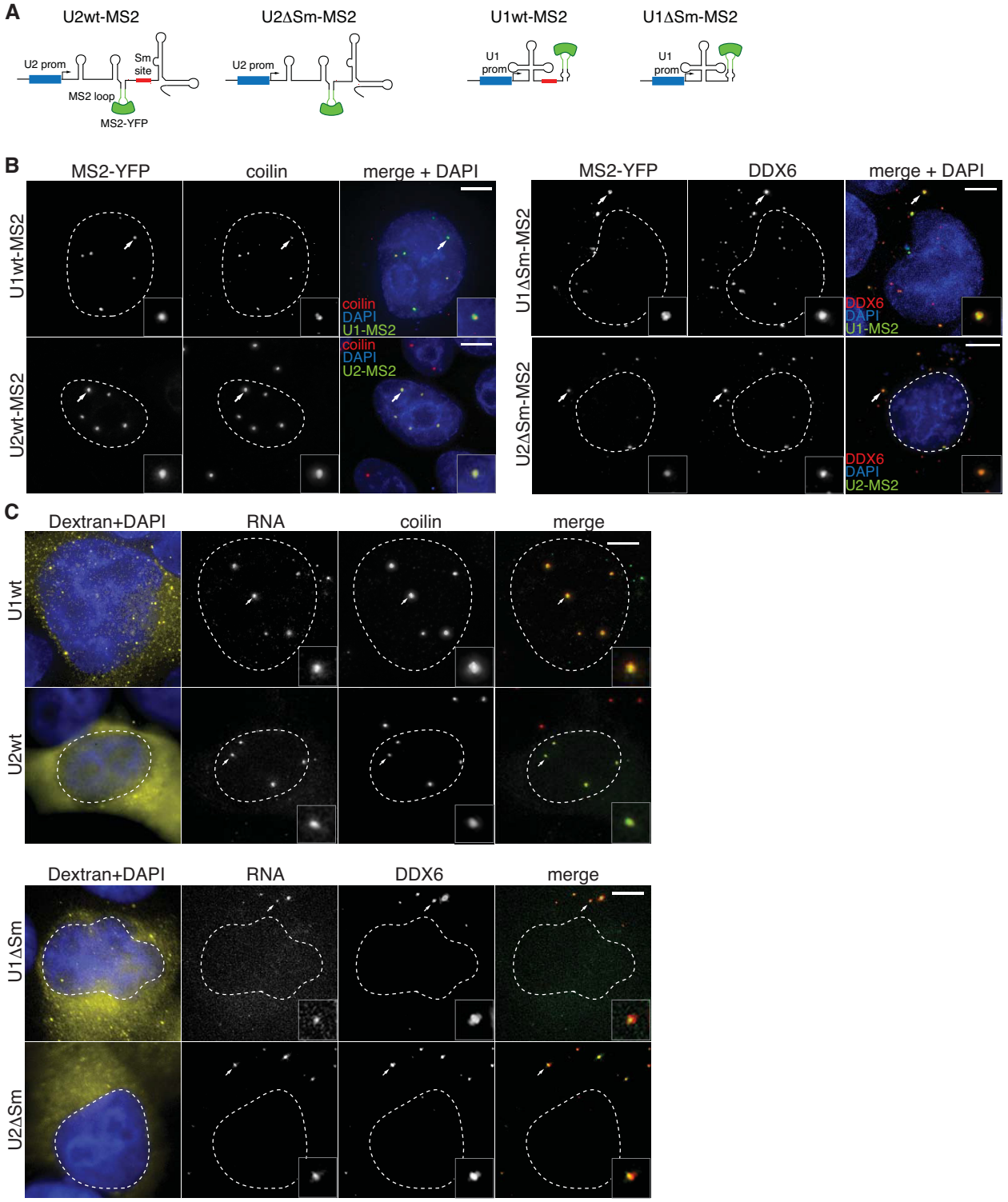

Figure 1. snRNAs with the Sm binding site localize to P-bodies. (**A**) The MS2 binding site was inserted into the U2 snRNA (stem loop IIb) and U1 snRNA (stem loop IV). Either full-length snRNAs or snRNAs lacking the Sm binding site were used for MS2 insertion. (**B**) MS2-tagged snRNAs were co-expressed with MS2-YFP protein and their localization in Cajal bodies (left panel) and P-bodies (right panel) was monitored. WT snRNAs localized to Cajal bodies, while deletion of the Sm motif retargeted ΔSm snRNAs into P-bodies. (**C**) *In vitro* transcribed snRNAs labeled with Alexa-488-UTP were microinjected into the cytoplasm of HeLa cells together with TRITC-labeled Dextran-70kDa (left panel; yellow). Dextran-70kDa does not cross the nuclear membrane and thus serves as a marker of cellular compartment where snRNAs were microinjected. In some cells, Dextran-70kDa accumulated in distinct cytoplasmic spots, and in a few cases these spots were localized next to P-bodies (see also Figure 3). Localization of WT snRNAs in Cajal bodies and ΔSm snRNAs in P-bodies was monitored. Cajal bodies were detected by indirect immunofluorescence of their marker coilin, and P-bodies by immunodetection of DDX6 (red). MS2-YFP and microinjected snRNAs were directly localized by fluorescence microscopy (green). DNA was labeled by DAPI (blue). Cajal bodies and P-bodies marked by arrows were magnified two times in insets. Bars represent 5 μm.

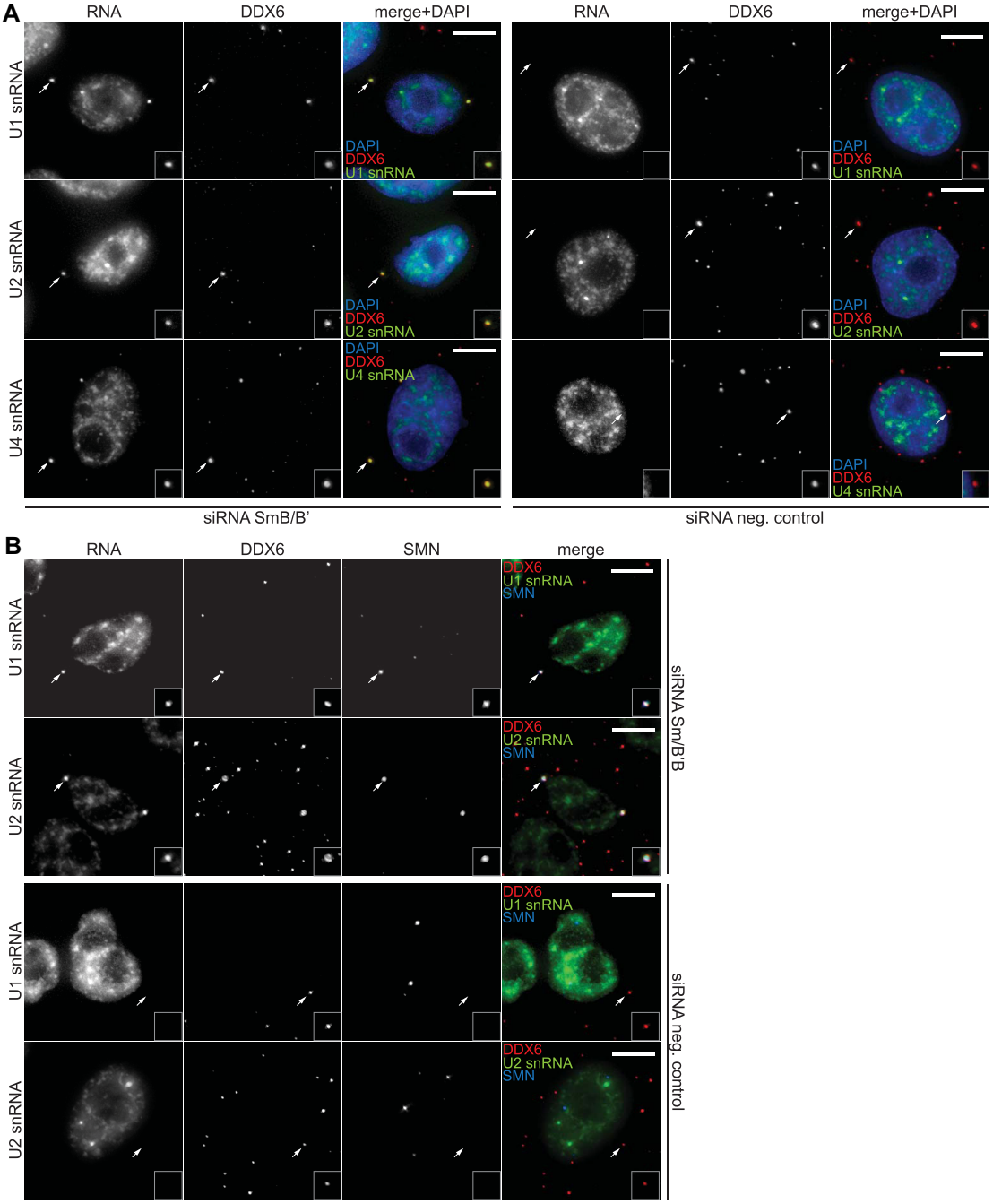

Figure 2. Knockdown of SmB/B′ protein induces snRNA localization to P-bodies. (**A**) SmB/B′ was downregulated by siRNA treatment and localization of snRNAs determined by *in situ* hybridization (green). P-bodies were visualized by immunodetection of DDX6 (red). DNA is labeled by DAPI (blue). (**B**) SmB/B′ was downregulated and snRNAs and DDX6 detected as in (**A**). SMN protein was localized by indirect immunofluorescence (blue). P-bodies marked by arrows were magnified two times in insets. Bars represent 5 μm.

SMN and Gemin5 are not essential for snRNA P-body localization

It has been suggested that the SMN complex, and specifically Gemin5, targets truncated snRNAs lacking the Sm site into P-bodies, likely via an interaction with the monomethyl 5′-cap (7,50). To test this hypothesis, we prepared U2 mutants lacking either the Sm site only (U2ΔSm) or lacking the Sm site together with stem loops III and IV at the 3′ end (U2ΔSmΔSMN). Stem loops III and IV were previously shown to interact with the SMN complex (31,53). Because Gemin5 specifically binds the Sm site and the 5′-monomethyl but not the trimethylated cap (6,7), we *in vitro* transcribed U2ΔSmΔSMN snRNA in the presence of the trimethylated cap analog ($m_3^{2,2,7}$G(5′)ppp(5′)G) to prevent binding of Gemin5. *In vitro* prepared snRNAs were microinjected into the cytoplasm and after 1 h incubation their localization in P-bodies was monitored. The snRNA lack-

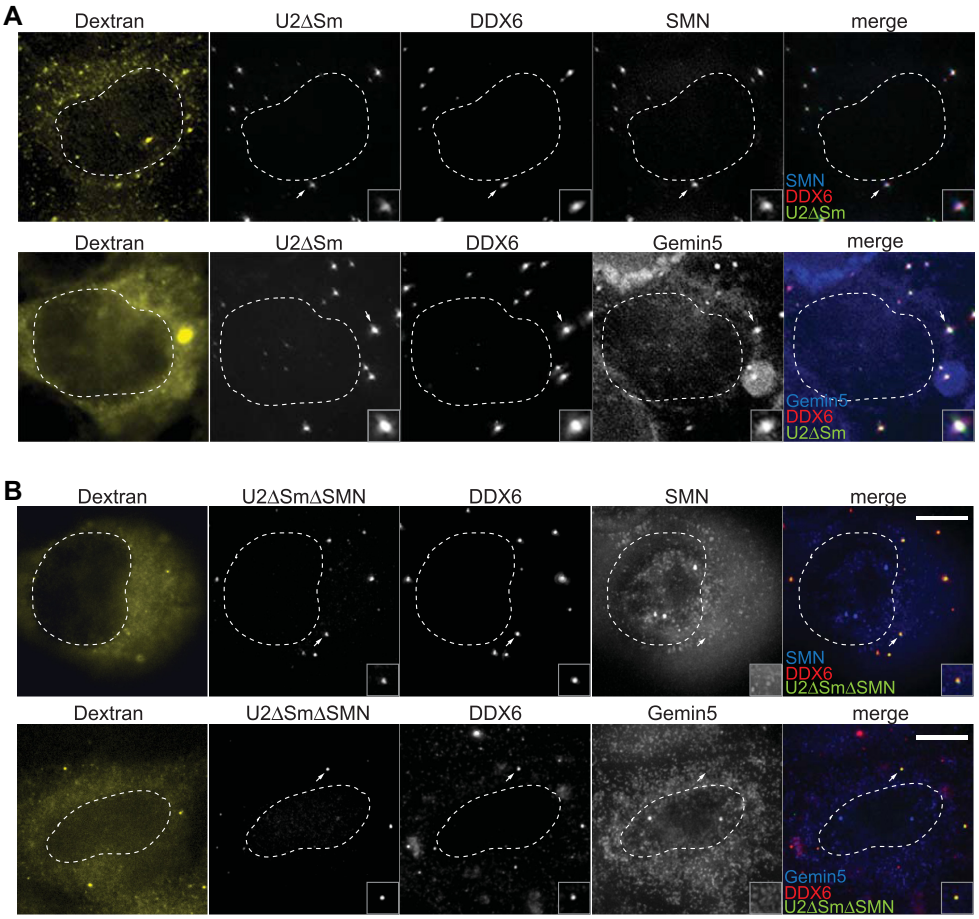

Figure 3. P-body localization of ΔSm snRNAs is SMN/Gemin5 independent. *In vitro* transcribed snRNAs labeled with Alexa-488-UTP (green) were microinjected into the cytoplasm of HeLa cells. The microinjection site was determined by co-injection of TRITC-Dextran-70kDa (yellow). snRNAs contain the trimethyl cap at the 5′ end and lack either (**A**) the Sm binding site (U2ΔSm) or (**B**) both the Sm and SMN binding sites (U2ΔSmΔSMN). DDX6 (red), a marker of P-bodies, SMN and Gemin5 (blue) were detected by indirect immunofluorescence. P-bodies marked by arrows were magnified two times in insets. Bars represent 5 μm.

ing both the Sm and SMN binding sites (U2ΔSmΔSMN) still localized to P-bodies. However, P-bodies that contained the U2ΔSmΔSMN snRNA did not accumulate either SMN or Gemin5 proteins, while both proteins localized in P-bodies positive for the U2ΔSm snRNA (Figure 3A and B). These results show that the 5′ monomethyl cap and Sm and SMN binding sites are not essential for P-body accumulation.

snRNAs lacking the Sm binding site are unstable

Next, we decided to identify factors that recognize defective snRNAs devoid of the Sm ring and target them to P-bodies. To determine proteins that interact with ΔSm snRNA, we co-transfected cells with U1-MS2 snRNA (either WT or ΔSm) and MS2-YFP and precipitated MS2-YFP-bound snRNPs by anti-GFP antibodies. However, U1ΔSm-MS2 snRNA was highly unstable and we were not able to isolate any detectable amount of U1ΔSm-MS2 snRNA (data not shown). The XRN1 exonuclease was suggested to degrade defective snRNAs (32). In order to stabilize ΔSm snRNA and characterize proteins bound to this defective snRNA, we decided to prevent ΔSm snRNA degradation by XRN1 and inserted an XRN1-resistant (xrRNA) sequence into U2 snRNA (54). The U2wt_xrRNA-MS2 RNA localized properly to Cajal bodies and U2ΔSm_xrRNA-MS2 to P-bodies (Supplementary Figure S5A). However, we did not observe any stabilization of the U2ΔSm_xrRNA-MS2 RNA, and only U2wt_xrRNA-MS2 snRNA was recovered after MS2-YFP immunoprecipitation (Supplementary Figure S5B).

Insertion of the xrRNA sequence did not stabilize snRNA without the Sm site, which suggests that additional degradation machineries are involved in ΔSm snRNA clearance. Therefore, we decided to concomitantly eliminate 5′→3′ and 3′→5′ cytoplasmic degradation machineries as another attempt to stabilize and characterize snRNPs without the Sm site. The knockout of 3′→5′ exonuclease DIS3L2 stabilized snRNA pseudogenes and snRNA precursors (20) and we speculated that DIS3L2 may also be involved in degradation of defective snRNAs lacking the Sm ring. Therefore, we expressed U1ΔSm-MS2 snRNA in DIS3L2 knockout (DIS3L2^{KO}) HEK cells (20) and reduced 5′→3′ degradation by RNAi-mediated depletion of XRN1 (Figure 4) or DCP2 (Supplementary Figure S6). In parallel, we expressed U1ΔSm-MS2 snRNA in DIS3L2^{KO}

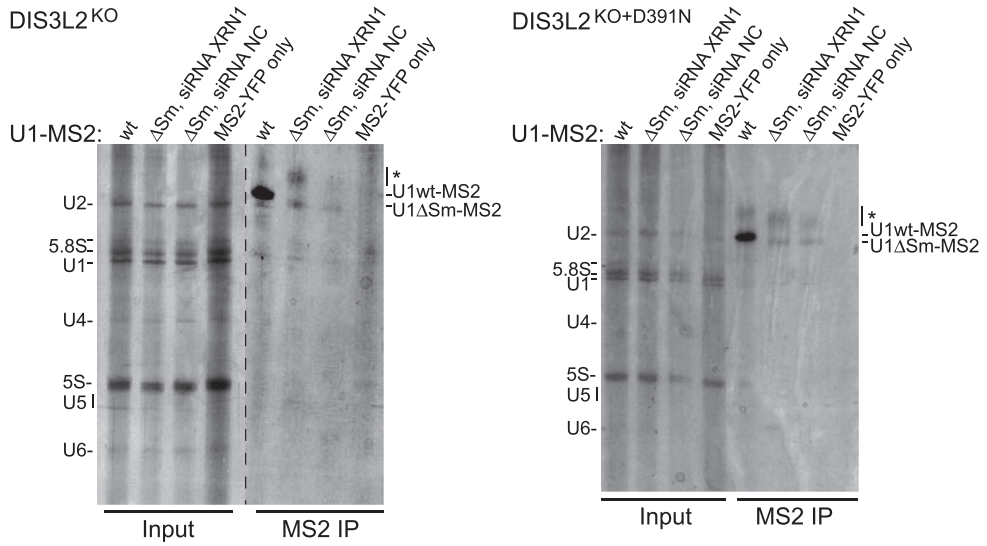

Figure 4. Deletion of the Sm site destabilizes U1 snRNA. U1wt-MS2 or U1ΔSm-MS2 were co-expressed with MS2-YFP in HEK293 DIS3L2^{KO} HEK cells (left panel) or DIS3L2^{KO} HEK cells conditionally expressing the catalytically inactive DIS3L2-D391N mutant (DIS3L2$^{KO+D391N}$, right panel). MS2-tagged snRNAs were immunoprecipitated via MS2-YFP, resolved in acrylamide UREA gels and silver stained. XRN1 protein was downregulated by RNAi. U1wt-MS2 was clearly visible after immunopurification, while only a weak signal was observed for U1ΔSm-MS2 snRNA even after knockdown of XRN1. Expression of MS2-YFP served as a negative control. Note a diffuse band migrating above mature U1 snRNAs (marked by an asterisk), which indicates non-templated 3′ end extension.

cells expressing the catalytically inactive DIS3L2 mutant (DIS3L2$^{KO+D391N}$), which was previously shown to stabilize extended precursors of snRNAs (20,21,55). We observed partial stabilization of U1ΔSm snRNA in both DIS3L2^{KO} and DIS3L2$^{KO+D391N}$ cell lines, which was further enhanced by downregulation of 5′→3′ degradation factors XRN1 and DCP2 (Figure 4 and Supplementary Figure S6). However, in neither case the amount of co-precipitated U1ΔSm-MS2 snRNA reached the level of WT U1-MS2 snRNA, and we were unable to characterize proteins co-precipitating with U1ΔSm-MS2 snRNA.

Sm ring-less snRNAs contain non-templated 3′ oligouridines and interact with DIS3L2

In both DIS3L2^{KO} and DIS3L2$^{KO+D391N}$ cell lines, we observed heterogeneous RNAs migrating above the mature U1-MS2 snRNA (marked by an asterisk in Figure 4), which indicates non-templated tailing as observed previously (20,21,37). To test whether episomally expressed snRNAs are targets of terminal uridylyl transferases (TUTases), we expressed U1wt-MS2 and U1ΔSm-MS2 T-REx-HeLa, isolated the fraction of short RNAs and analyzed 3′ ends of several clones derived from isolated RNAs by RACE using MS2-specific primers (Figure 5A). Non-templated uridines were detected in the majority of the U1ΔSm-MS2 clones, while only one of the WT clones contained untemplated 3′ oligo(U) extensions. To analyze whether episomally expressed snRNAs are recognized by DIS3L2, we expressed both U1 and U2 variants without the Sm site in the DIS3L2$^{KO+D391N}$ cell line. Catalytically inactive DIS3L2^{D391N}, which contained the FLAG peptide, was then immunoprecipitated by the anti-FLAG antibody (Supplementary Figure S7A) and the bound snRNAs were analyzed using MS2-specific and 3′ end linker-specific primers to detect only the episomally expressed snRNAs (Figure 5B). Both WT and ΔSm snRNAs co-purified with Flag-DIS3L2^{D391N}, which shows that under these conditions DIS3L2 interacts with both WT and defective snRNAs lacking the Sm motif.

To analyze the presence of non-templated oligo(U) at the 3′ end of DIS3L2-bound snRNAs, we expressed WT and ΔSm-MS2 snRNAs in the DIS3L2$^{KO+D391N}$ T-REx-HeLa cell line, immunoprecipitated Flag-DIS3L2^{D391N} and sequenced several clones derived from co-precipitated snRNAs (Figure 6). The results revealed the presence of oligo(U) at the 3′ end of both WT and ΔSm snRNAs. Deletion of the Sm site enhanced the 3′ uridylation of U1 snRNA and inhibited correct trimming of the U2 3′ termini. Downregulation of XRN1 by RNAi did not influence the level or oligo(U) outcome of U1 snRNA (Supplementary Figure S7B and Figure 5B). Together, these results show that snRNAs lacking the Sm site are uridylated and that DIS3L2 binds these snRNAs.

LSm1 protein is involved in P-body targeting of snRNAs without the Sm ring

However, the association of ΔSm snRNAs with DIS3L2 does not explain why snRNAs without the Sm ring accumulate in P-bodies, because human DIS3L2 is not accumulated in these cytoplasmic structures but is rather dispersed throughout the cytoplasm (56). Potential candidates for ΔSm snRNA targeting to P-bodies are LSm proteins 1–7, which localize to P-bodies and strongly bind oligo(U) (46,57). To test whether LSm1–7 proteins interact with WT snRNAs lacking the Sm ring, we knocked down the SmB/B′ protein and transiently expressed LSm1-GFP. Next, we performed immunoprecipitation using anti-GFP antibodies and analyzed snRNAs co-precipitated with LSm1-GFP

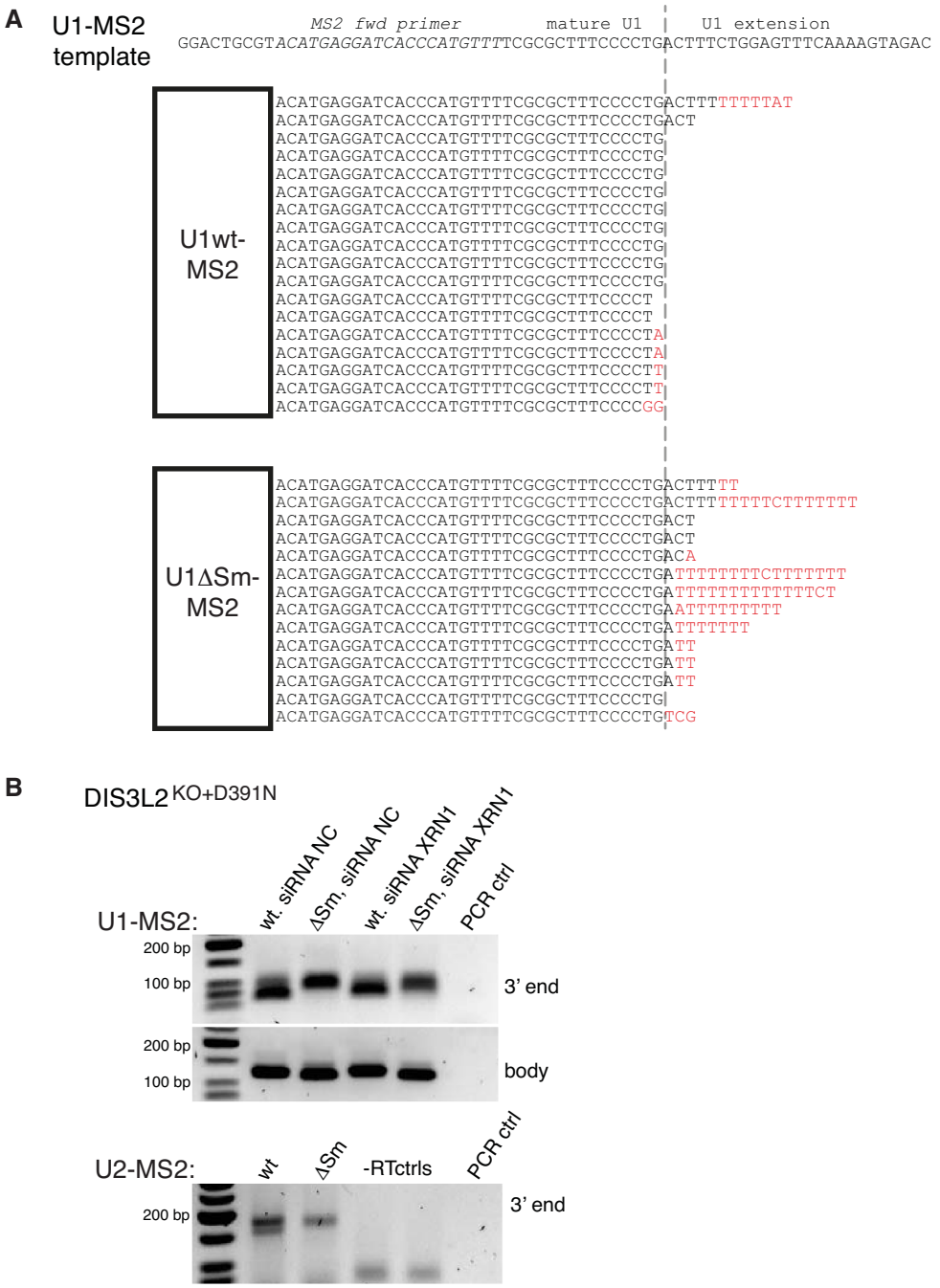

Figure 5. snRNAs without the Sm site contain improperly processed oligouridylated 3′ ends. (**A**) The WT and Sm mutant U1 snRNAs (U1wt-MS2 and U1ΔSm-MS2, as in Figure 4) were transiently expressed in Hela cells and their 3′ ends were analyzed by RT-PCR and sequencing using the 3′ end linker-specific and MS2-specific primers (as indicated in the scheme on top). The untemplated nucleotides are marked in red. (**B**) Catalytically inactive DIS3L2^{D391N} interacts with WT and ΔSm snRNAs. RT-PCR analysis of U1 and U2 WT and ΔSm U1 and U2 snRNAs episomally expressed in genetically modified HeLa cells expressing only catalytically inactive DIS3L2 (DIS3L2$^{KO+D391N}$) in the presence of either control non-targeting siRNAs (siRNA NC) or siRNAs targeting *XRN1* mRNA (siRNA XRN1). The upper panel (3′ end) for U1-MS2 snRNA shows PCR products using 3′ end linker and MS2 primers. The lower panel (body) shows PCR products obtained with MS2 and U1 snRNA gene-specific reverse primer. PCR ctrl is a control without any cDNA. -RT is a control where no reverse transcriptase was added in the RT step of the reaction.

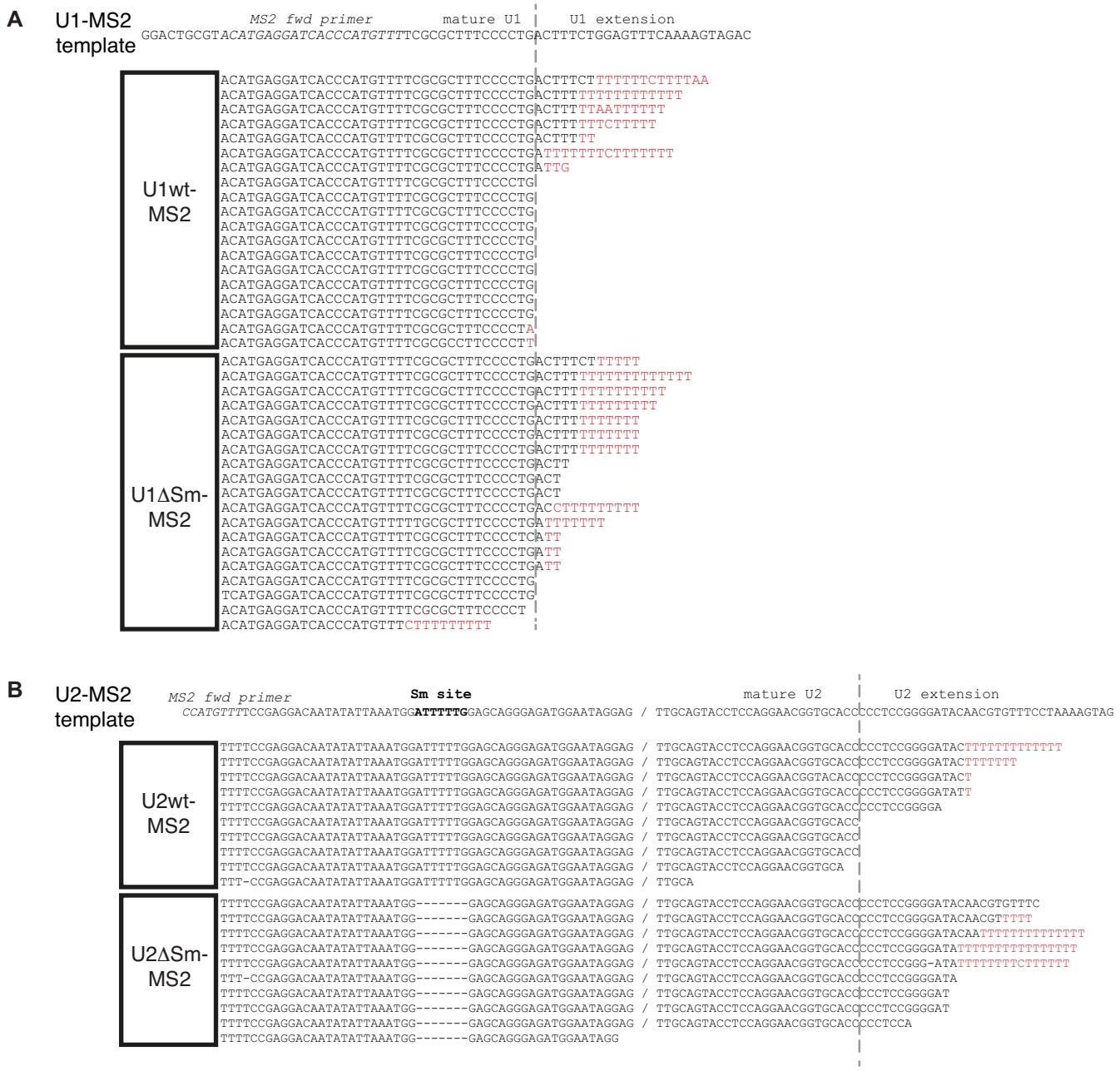

Figure 6. DIS3L2^{D391N} binds oligouridylated snRNAs. (**A**) WT and ΔSm-MS2 U1 snRNAs (U1wt-MS2 and U1ΔSm-MS2) and (**B**) WT and ΔSm-MS2 U2 snRNAs (U2wt-MS2 and U2ΔSm-MS2) were episomally expressed in the DIS3L2$^{KO+D391N}$ T-REx-HeLa cell line. RNAs co-precipitated with Flag-DIS3L2^{D391N} were analyzed by RT-PCR and sequenced using MS2-specific and 3′ end linker-specific primers. The sequencing results are aligned and the scheme above shows the regions corresponding to the mature snRNAs and, wherever detected, also the regions corresponding to 3′ terminal encoded extensions of U1 or U2 snRNAs. The post-transcriptionally added non-templated oligonucleotides (oligo(Us)) are marked in red. The dashed lines in U2ΔSm-MS2 sample depict the Sm site deletion.

by RT-qPCR (Figure 7A and Supplementary Figure S7C). Under physiological conditions, the association of LSm1-GFP with snRNAs was negligible. However, downregulation of SmB/B′ enhanced association of all snRNAs (except the U6 snRNA) with LSm1-GFP. Next, we tested whether the LSm1 protein is important for localization of snRNAs without the Sm ring into P-bodies. We concomitantly downregulated LSm1 and SmB/B′ and detected endogenous U2 snRNA by *in situ* hybridization (Figure 7B). In parallel, we downregulated LSm1 and transiently expressed U2ΔSm-MS2 snRNA lacking the Sm site (Figure 7C). Reduction of LSm1 expression partially lowered the number P-bodies per cell as described previously (58), but in both cases the knockdown of LSm1 reduced localization of U2 snRNA without the Sm ring in the P-bodies. These data strongly indicate that the LSm1–7 proteins are involved in targeting snRNAs devoid of the Sm ring into these cytoplasmic structures.

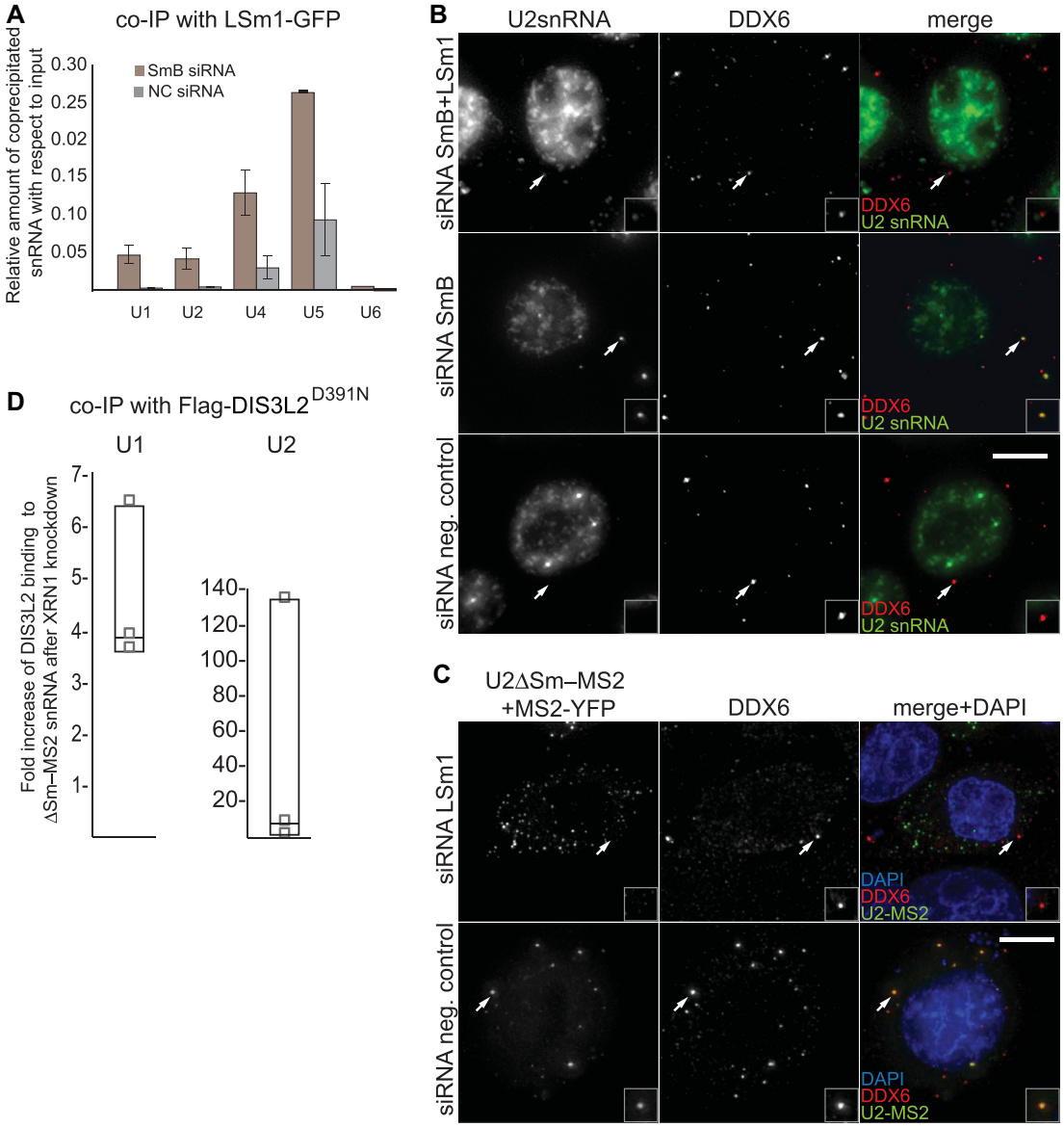

Figure 7. Lsm1 protein interacts with ΔSm snRNAs and targets them to P-bodies. (**A**) Sm ring formation was inhibited by knockdown of SmB/B′ and the interaction of snRNAs with LSm1-GFP was assayed by Lsm1-GFP immunoprecipitation followed by RT-qPCR. The amount of co-precipitated snRNAs was normalized to input. NC siRNA: negative control siRNA. (**B**) Sm ring formation was inhibited by knockdown of SmB/B′ and the localization of endogenous U2 snRNA was assayed by *in situ* hybridization (green) before or after the treatment with siRNA against LSm1. (**C**) P-body accumulation of U2ΔSm snRNA after the knockdown of LSm1 was monitored by MS2-YFP (green). P-body marker DDX6 was visualized by indirect immunofluorescence (red). DNA was stained by DAPI (blue). P-bodies marked by arrows are magnified two times in insets. Bars represent 5 μm. (**D**) U1ΔSm-MS2 and U2ΔSm-MS2 were expressed in DIS3L2$^{KO+D391N}$ cells, XRN1 was downregulated by siRNA and Flag-DIS3L2^{D391N} expression was induced by doxycycline. snRNAs co-precipitated with Flag-DIS3L2^{D391N} analyzed by RT-qPCR with primers specific to the MS2 tag. The amount of snRNAs precipitated after XRN1 knockdown was normalized to snRNAs precipitated from cells treated with negative control siRNA. Box plot shows three independent experiments.

Our results show that both DIS3L2 and LSm1 proteins interact with Sm ring-less snRNAs. To test whether different degradation machineries compete for snRNA substrates, we mapped the interaction of U1 and U2 ΔSm snRNAs with DIS3L2^{D391N} after downregulation of XRN1 (Figure 7D). In both cases, the knockdown of XRN1 increased immunoprecipitation of defective snRNAs with Flag-DIS3L2^{D391N}, indicating that inhibition of a 5′→3′ degradation pathway redirects snRNAs to the 3′→5′ degradation machinery.

DISCUSSION

Cells utilize several control mechanisms to ensure that only properly assembled snRNPs reach the nucleoplasm and are embedded into the spliceosome. Results from human cell culture and yeast indicate that a failure of quality control negatively affects cell growth and splicing (18,59). Here, we studied a cytoplasmic control mechanism that detects snRNAs without the Sm ring and directs them to P-bodies. We provide evidence that P-body targeting is independent of SMN complex components, but requires the LSm1 pro-

tein and likely the whole LSm1–7 ring, because deletion of LSm1 causes re-localization of other LSm proteins to the cell nucleus (58).

Deletion of the Sm site induces degradation of ΔSm snRNAs, indicating that human somatic cells are able to efficiently recognize and cleave defective snRNAs. This is in contrast *to Xenopus laevis* oocytes, where injected ΔSm snRNAs were stable for several hours (24). However, RNAs are generally more stable in oocytes, partially due to the low activity of enzymes involved in RNA degradation (60,61), which might explain the discrepancy in snRNA stability between somatic cells and oocytes.

In search for the snRNA degradation machinery, we observed increased 3′ end uridylation of specifically snRNAs lacking the Sm site (Figure 5). Further analyses revealed that uridylated ΔSm U1 and U2 snRNAs are bound by the catalytically dead DIS3L2 mutant DIS3L2 ($DIS3L2^{D391N}$) (Figure 6). These data provide direct evidence that at least a fraction of U1 and U2 snRNAs without the Sm ring are uridylated and degraded by the TUT-DIS3L2 surveillance pathway. DIS3L2 thus emerges as the key cytoplasmic 3′→5′ nuclease that degrades various non-coding RNAs, including short and defective snRNAs lacking the Sm ring (this study), read-through snRNA transcripts including snRNA pseudogenes, miRNAs and RNA polymerase III transcripts (20–22,51,55,62).

However, the fact that ΔSm U1-MS2 snRNA was unstable in $DIS3L2^{KO}$ cells indicates that alternative degradation pathways act to clear non-functional snRNAs. Human XRN1 has been suggested to degrade a truncated form of U1 snRNA, and ∼1.6-fold stabilization of U1 with mutated Sm site was observed upon XRN1 knockdown (32). Consistently, we observed partial stabilization of U1ΔSm-MS2 snRNA in $DIS3L2^{KO}$ cells after XRN1 and DCP2 downregulation (Figure 4 and Supplementary Figure S5). In addition, downregulation of the SmB/B′ protein enhanced association of snRNAs with LSm1 (Figure 7), a protein involved in XRN1-mediated decay, which indicates a direct association between snRNAs lacking the Sm ring and XRN1-linked machinery (63–65). Together, these data indicate that XRN1 is involved in clearance of defective snRNAs.

However, even after the knockdown of XRN1 and DCP2, the amount of isolated U1ΔSm-MS2 snRNA was much lower than that of U1wt-MS2 (Figure 4 and Supplementary Figure S5). Consistently, insertion of the XRN1-resistant sequence into U2ΔSm snRNA (U2ΔSm_xrRNA-MS2) did not significantly stabilize this snRNA (Supplementary Figure S5). While we cannot completely exclude that the remaining XRN1 activity after siRNA treatment is still able to degrade ΔSm snRNAs, we speculate that alternative degradation pathway(s) and enzymes, e.g. the exosome, histone mRNA targeting ERI1 and the U6 snRNA processing enzyme USB1 (35,36,66), can fill in and cleave ΔSm snRNAs when DIS3L2/XRN1 are inactive. In addition, the 5′→3′ decay pathway plays a significant role in the cytoplasmic RNA decay, and other enzymatic activities such as the 5′-hydroxyl dinucleotide hydrolase and 5′→3′ exoribonuclease activity of the DXO/Rai1 family of enzymes may contribute to the snRNA surveillance (67).

What is the role of P-bodies in snRNA surveillance? Recent data suggest that P-bodies are not primary sites of mRNA degradation, but rather reservoirs for transcriptionally silenced mRNA (65,68–71). Applying this concept to non-coding RNAs, the accumulation of defective snRNAs in P-bodies should not be viewed as a step toward their degradation, but rather as their sequestration from the cytoplasm to prolong a time window for assembly of the Sm ring. Consistent with this hypothesis, the Sm ring assembly machinery co-migrates to P-bodies with snRNAs after inhibition of Sm ring formation by either SmB/B′ knockdown (Figure 2) or microinjection of U2ΔSm snRNA (Figure 3). However, in contrast to previous suggestions (7,50), our data indicate that defective snRNAs accumulate in P-bodies independently of SMN and Gemin5 proteins and rather suggest that the SMN complex piggybacks to P-bodies on snRNAs. Instead, we provide evidence that the LSm1 protein, and likely the whole LSm1–7 ring, is essential for P-body localization of Sm ring-less snRNAs. LSm1–7 proteins thus represent an important component of the snRNA surveillance pathway in the cytoplasm. We propose a model where snRNAs that fail to acquire the Sm ring are uridylated at the 3′ end and are either degraded by DIS3L2 (or alternative degradation machinery) or bound by LSm1–7 proteins and sequestered together with the SMN complex to P-bodies, where Sm ring formation can be completed or snRNAs are degraded by XRN1.

SUPPLEMENTARY DATA

Supplementary Data are available at NAR Online.

ACKNOWLEDGEMENTS

The authors thank Tomas Pis for the preparation of the stable HeLa $DIS3L2^{KO}$ and $DIS3L2^{KO+D391N}$ cell lines, Karolina Vavrouskova for excellent technical support and Franco Pagani (Human Molecular Genetics, International Centre for Genetic Engineering and Biotechnology, Trieste, Italy) for plasmids. The authors also acknowledge the Light Microscopy Core Facility, IMG CAS, Prague, Czech Republic.

FUNDING

Czech Science Foundation [18-10035S to D.S., 16-21341S and 20-19617S to Š.V.]; Czech Academy of Sciences [RVO68378050]; Central European Institute of Technology [LQ1601]; Grant Agency of Charles University [134516 to A.R.]; Ministry of Education, Youth and Sports of the Czech Republic [LM2015062]. Funding for open access charge: Czech Science Foundation.
Conflict of interest statement. None declared.

REFERENCES

1. Houry,W.A., Bertrand,E. and Coulombe,B. (2018) The PAQosome, an R2TP-based chaperone for quaternary structure formation. *Trends Biochem. Sci.*, **43**, 4–9.
2. Gruss,O.J., Meduri,R., Schilling,M. and Fischer,U. (2017) UsnRNP biogenesis: mechanisms and regulation. *Chromosoma*, **126**, 577–593.

3. Li,D.K., Tisdale,S., Lotti,F. and Pellizzoni,L. (2014) SMN control of RNP assembly: from post-transcriptional gene regulation to motor neuron disease. *Semin. Cell Dev. Biol.*, **32**, 22–29.
4. Raimer,A.C., Gray,K.M. and Matera,A.G. (2017) SMN: a chaperone for nuclear RNP social occasions? *RNA Biol.*, **14**, 701–711.
5. Golembe,T.J., Yong,J. and Dreyfuss,G. (2005) Specific sequence features, recognized by the SMN complex, identify snRNAs and determine their fate as snRNPs. *Mol. Cell. Biol.*, **25**, 10989–11004.
6. Jin,W., Wang,Y., Liu,C.P., Yang,N., Jin,M., Cong,Y., Wang,M. and Xu,R.M. (2016) Structural basis for snRNA recognition by the double-WD40 repeat domain of Gemin5. *Genes Dev.*, **30**, 2391–2403.
7. Xu,C., Ishikawa,H., Izumikawa,K., Li,L., He,H., Nobe,Y., Yamauchi,Y., Shahjee,H.M., Wu,X.H., Yu,Y.T. *et al.* (2016) Structural insights into Gemin5-guided selection of pre-snRNAs for snRNP assembly. *Genes Dev.*, **30**, 2376–2390.
8. Neuenkirchen,N., Englbrecht,C., Ohmer,J., Ziegenhals,T., Chari,A. and Fischer,U. (2015) Reconstitution of the human U snRNP assembly machinery reveals stepwise Sm protein organization. *EMBO J.*, **34**, 1925–1941.
9. Pellizzoni,L., Yong,J. and Dreyfuss,G. (2002) Essential role for the SMN complex in the specificity of snRNP assembly. *Science*, **298**, 1775–1779.
10. Chari,A., Golas,M.M., Klingenhager,M., Neuenkirchen,N., Sander,B., Englbrecht,C., Sickmann,A., Stark,H. and Fischer,U. (2008) An assembly chaperone collaborates with the SMN complex to generate spliceosomal snRNPs. *Cell*, **135**, 497–509.
11. Grimm,C., Chari,A., Pelz,J.P., Kuper,J., Kisker,C., Diederichs,K., Stark,H., Schindelin,H. and Fischer,U. (2013) Structural basis of assembly chaperone-mediated snRNP formation. *Mol. Cell*, **49**, 692–703.
12. Stanek,D. (2017) Cajal bodies and snRNPs: friends with benefits. *RNA Biol.*, **14**, 671–679.
13. Jady,B.E., Darzacq,X., Tucker,K.E., Matera,A.G., Bertrand,E. and Kiss,T. (2003) Modification of Sm small nuclear RNAs occurs in the nucleoplasmic Cajal body following import from the cytoplasm. *EMBO J.*, **22**, 1878–1888.
14. Stanek,D. and Neugebauer,K.M. (2004) Detection of snRNP assembly intermediates in Cajal bodies by fluorescence resonance energy transfer. *J. Cell Biol.*, **166**, 1015–1025.
15. Bizarro,J., Dodre,M., Huttin,A., Charpentier,B., Schlotter,F., Branlant,C., Verheggen,C., Massenet,S. and Bertrand,E. (2015) NUFIP and the HSP90/R2TP chaperone bind the SMN complex and facilitate assembly of U4-specific proteins. *Nucleic Acids Res.*, **43**, 8973–8989.
16. Malinova,A., Cvackova,Z., Mateju,D., Horejsi,Z., Abeza,C., Vandermoere,F., Bertrand,E., Stanek,D. and Verheggen,C. (2017) Assembly of the U5 snRNP component PRPF8 is controlled by the HSP90/R2TP chaperones. *J. Cell Biol.*, **216**, 1579–1596.
17. Cloutier,P., Poitras,C., Durand,M., Hekmat,O., Fiola-Masson,E., Bouchard,A., Faubert,D., Chabot,B. and Coulombe,B. (2017) R2TP/Prefoldin-like component RUVBL1/RUVBL2 directly interacts with ZNHIT2 to regulate assembly of U5 small nuclear ribonucleoprotein. *Nat. Commun.*, **8**, 15615.
18. Novotny,I., Malinova,A., Stejskalova,E., Mateju,D., Klimesova,K., Roithova,A., Sveda,M., Knejzlik,Z. and Stanek,D. (2015) SART3-dependent accumulation of incomplete spliceosomal snRNPs in Cajal bodies. *Cell Rep.*, **10**, 429–440.
19. Baillat,D., Hakimi,M.A., Nr,A.M., Shilatifard,A., Cooch,N. and Shiekhattar,R. (2005) Integrator, a multiprotein mediator of small nuclear RNA processing, associates with the C-terminal repeat of RNA polymerase II. *Cell*, **123**, 265–276.
20. Ustianenko,D., Pasulka,J., Feketova,Z., Bednarik,L., Zigackova,D., Fortova,A., Zavolan,M. and Vanacova,S. (2016) TUT-DIS3L2 is a mammalian surveillance pathway for aberrant structured non-coding RNAs. *EMBO J.*, **35**, 2179–2191.
21. Labno,A., Warkocki,Z., Kulinski,T., Krawczyk,P.S., Bijata,K., Tomecki,R. and Dziembowski,A. (2016) Perlman syndrome nuclease DIS3L2 controls cytoplasmic non-coding RNAs and provides surveillance pathway for maturing snRNAs. *Nucleic Acids Res.*, **44**, 10437–10453.
22. Pirouz,M., Du,P., Munafo,M. and Gregory,R.I. (2016) Dis3l2-mediated decay is a quality control pathway for noncoding RNAs. *Cell Rep.*, **16**, 1861–1873.
23. Machyna,M., Kehr,S., Straube,K., Kappei,D., Buchholz,F., Butter,F., Ule,J., Hertel,J., Stadler,P.F. and Neugebauer,K.M. (2014) The coilin interactome identifies hundreds of small noncoding RNAs that traffic through Cajal bodies. *Mol. Cell*, **56**, 389–399.
24. Suzuki,T., Izumi,H. and Ohno,M. (2010) Cajal body surveillance of U snRNA export complex assembly. *J. Cell Biol.*, **190**, 603–612.
25. Smith,K.P. and Lawrence,J.B. (2000) Interactions of U2 gene loci and their nuclear transcripts with Cajal (coiled) bodies: evidence for PreU2 within Cajal bodies. *Mol. Biol. Cell*, **11**, 2987–2998.
26. Massenet,S., Pellizzoni,L., Paushkin,S., Mattaj,I.W. and Dreyfuss,G. (2002) The SMN complex is associated with snRNPs throughout their cytoplasmic assembly pathway. *Mol. Cell. Biol.*, **22**, 6533–6541.
27. Prusty,A.B., Meduri,R., Prusty,B.K., Vanselow,J., Schlosser,A. and Fischer,U. (2017) Impaired spliceosomal UsnRNP assembly leads to Sm mRNA down-regulation and Sm protein degradation. *J. Cell Biol.*, **216**, 2391–2407.
28. Paknia,E., Chari,A., Stark,H. and Fischer,U. (2016) The ribosome cooperates with the assembly chaperone pICln to initiate formation of snRNPs. *Cell Rep.*, **16**, 3103–3112.
29. Fischer,U., Sumpter,V., Sekine,M., Satoh,T. and Luhrmann,R. (1993) Nucleo-cytoplasmic transport of U snRNPs: definition of a nuclear location signal in the Sm core domain that binds a transport receptor independently of the m3G cap. *EMBO J.*, **12**, 573–583.
30. Malatesta,M., Fakan,S. and Fischer,U. (1999) The Sm core domain mediates targeting of U1 snRNP to subnuclear compartments involved in transcription and splicing. *Exp. Cell Res.*, **249**, 189–198.
31. Roithova,A., Klimesova,K., Panek,J., Will,C.L., Luhrmann,R., Stanek,D. and Girard,C. (2018) The Sm-core mediates the retention of partially-assembled spliceosomal snRNPs in Cajal bodies until their full maturation. *Nucleic Acids Res.*, **46**, 3774–3790.
32. Shukla,S. and Parker,R. (2014) Quality control of assembly-defective U1 snRNAs by decapping and 5′-to-3′ exonucleolytic digestion. *Proc. Natl Acad. Sci. U.S.A.*, **111**, E3277–E3286.
33. Ishikawa,H., Nobe,Y., Izumikawa,K., Yoshikawa,H., Miyazawa,N., Terukina,G., Kurokawa,N., Taoka,M., Yamauchi,Y., Nakayama,H. *et al.* (2014) Identification of truncated forms of U1 snRNA reveals a novel RNA degradation pathway during snRNP biogenesis. *Nucleic Acids Res.*, **42**, 2708–2724.
34. Labno,A., Tomecki,R. and Dziembowski,A. (2016) Cytoplasmic RNA decay pathways: enzymes and mechanisms. *Biochim. Biophys. Acta*, **1863**, 3125–3147.
35. Hoefig,K.P., Rath,N., Heinz,G.A., Wolf,C., Dameris,J., Schepers,A., Kremmer,E., Ansel,K.M. and Heissmeyer,V. (2013) Eri1 degrades the stem-loop of oligouridylated histone mRNAs to induce replication-dependent decay. *Nat. Struct. Mol. Biol.*, **20**, 73–81.
36. Nomura,Y., Roston,D., Montemayor,E.J., Cui,Q. and Butcher,S.E. (2018) Structural and mechanistic basis for preferential deadenylation of U6 snRNA by Usb1. *Nucleic Acids Res.*, **46**, 11488–11501.
37. Ishikawa,H., Nobe,Y., Izumikawa,K., Taoka,M., Yamauchi,Y., Nakayama,H., Simpson,R.J., Isobe,T. and Takahash,N. (2018) Truncated forms of U2 snRNA (U2-tfs) are shunted toward a novel uridylylation pathway that differs from the degradation pathway for U1-tfs. *RNA Biol.*, **15**, 261–268.
38. van Dijk,E., Cougot,N., Meyer,S., Babajko,S., Wahle,E. and Seraphin,B. (2002) Human Dcp2: a catalytically active mRNA decapping enzyme located in specific cytoplasmic structures. *EMBO J.*, **21**, 6915–6924.
39. Wang,Z., Jiao,X., Carr-Schmid,A. and Kiledjian,M. (2002) The hDcp2 protein is a mammalian mRNA decapping enzyme. *Proc. Natl Acad. Sci. U.S.A.*, **99**, 12663–12668.
40. Bouveret,E., Rigaut,G., Shevchenko,A., Wilm,M. and Seraphin,B. (2000) A Sm-like protein complex that participates in mRNA degradation. *EMBO J.*, **19**, 1661–1671.
41. Song,M.G. and Kiledjian,M. (2007) 3′ Terminal oligo U-tract-mediated stimulation of decapping. *RNA*, **13**, 2356–2365.
42. Totaro,A., Renzi,F., La Fata,G., Mattioli,C., Raabe,M., Urlaub,H. and Achsel,T. (2011) The human Pat1b protein: a novel mRNA deadenylation factor identified by a new immunoprecipitation technique. *Nucleic Acids Res.*, **39**, 635–647.
43. Tharun,S., He,W., Mayes,A.E., Lennertz,P., Beggs,J.D. and Parker,R. (2000) Yeast Sm-like proteins function in mRNA decapping and decay. *Nature*, **404**, 515–518.

44. Wu,D., Muhlrad,D., Bowler,M.W., Jiang,S., Liu,Z., Parker,R. and Song,H. (2014) Lsm2 and Lsm3 bridge the interaction of the Lsm1–7 complex with Pat1 for decapping activation. *Cell Res.*, **24**, 233–246.
45. Chowdhury,A., Mukhopadhyay,J. and Tharun,S. (2007) The decapping activator Lsm1p-7p–Pat1p complex has the intrinsic ability to distinguish between oligoadenylated and polyadenylated RNAs. *RNA*, **13**, 998–1016.
46. Zhou,L., Zhou,Y., Hang,J., Wan,R., Lu,G., Yan,C. and Shi,Y. (2014) Crystal structure and biochemical analysis of the heptameric Lsm1–7 complex. *Cell Res.*, **24**, 497–500.
47. Sobti,M., Cubeddu,L., Haynes,P.A. and Mabbutt,B.C. (2010) Engineered rings of mixed yeast Lsm proteins show differential interactions with translation factors and U-rich RNA. *Biochemistry*, **49**, 2335–2345.
48. Tharun,S. and Parker,R. (2001) Targeting an mRNA for decapping: displacement of translation factors and association of the Lsm1p-7p complex on deadenylated yeast mRNAs. *Mol. Cell*, **8**, 1075–1083.
49. Hrossova,D., Sikorsky,T., Potesil,D., Bartosovic,M., Pasulka,J., Zdrahal,Z., Stefl,R. and Vanacova,S. (2015) RBM7 subunit of the NEXT complex binds U-rich sequences and targets 3′-end extended forms of snRNAs. *Nucleic Acids Res.*, **43**, 4236–4248.
50. Jiang,D., Zou,X., Zhang,C., Chen,J., Li,Z., Wang,Y., Deng,Z., Wang,L. and Chen,S. (2018) Gemin5 plays a role in unassembled-U1 snRNA disposal in SMN-deficient cells. *FEBS Lett.*, **592**, 1400–1411.
51. Ustianenko,D., Hrossova,D., Potesil,D., Chalupnikova,K., Hrazdilova,K., Pachernik,J., Cetkovska,K., Uldrijan,S., Zdrahal,Z. and Vanacova,S. (2013) Mammalian DIS3L2 exoribonuclease targets the uridylated precursors of let-7 miRNAs. *RNA*, **19**, 1632–1638.
52. Huranova,M., Hnilicova,J., Fleischer,B., Cvackova,Z. and Stanek,D. (2009) A mutation linked to retinitis pigmentosa in HPRP31 causes protein instability and impairs its interactions with spliceosomal snRNPs. *Hum. Mol. Genet.*, **18**, 2014–2023.
53. Yong,J., Golembe,T.J., Battle,D.J., Pellizzoni,L. and Dreyfuss,G. (2004) snRNAs contain specific SMN-binding domains that are essential for snRNP assembly. *Mol. Cell. Biol.*, **24**, 2747–2756.
54. Chapman,E.G., Moon,S.L., Wilusz,J. and Kieft,J.S. (2014) RNA structures that resist degradation by Xrn1 produce a pathogenic dengue virus RNA. *eLife*, **3**, e01892.
55. Eckwahl,M.J., Sim,S., Smith,D., Telesnitsky,A. and Wolin,S.L. (2015) A retrovirus packages nascent host noncoding RNAs from a novel surveillance pathway. *Genes Dev.*, **29**, 646–657.
56. Lubas,M., Damgaard,C.K., Tomecki,R., Cysewski,D., Jensen,T.H. and Dziembowski,A. (2013) Exonuclease hDIS3L2 specifies an exosome-independent 3′–5′ degradation pathway of human cytoplasmic mRNA. *EMBO J.*, **32**, 1855–1868.
57. Ingelfinger,D., Arndt-Jovin,D.J., Luhrmann,R. and Achsel,T. (2002) The human LSm1–7 proteins colocalize with the mRNA-degrading enzymes Dcp1/2 and Xrnl in distinct cytoplasmic foci. *RNA*, **8**, 1489–1501.
58. Novotny,I., Podolska,K., Blazikova,M., Valasek,L.S., Svoboda,P. and Stanek,D. (2012) Nuclear LSm8 affects number of cytoplasmic processing bodies via controlling cellular distribution of Like-Sm proteins. *Mol. Biol. Cell*, **23**, 3776–3785.
59. Becker,D., Hirsch,A.G., Bender,L., Lingner,T., Salinas,G. and Krebber,H. (2019) Nuclear pre-snRNA export is an essential quality assurance mechanism for functional spliceosomes. *Cell Rep.*, **27**, 3199–3214.
60. Ma,J., Flemr,M., Strnad,H., Svoboda,P. and Schultz,R.M. (2013) Maternally recruited DCP1A and DCP2 contribute to messenger RNA degradation during oocyte maturation and genome activation in mouse. *Biol. Reprod.*, **88**, 11.
61. Ma,J., Fukuda,Y. and Schultz,R.M. (2015) Mobilization of dormant Cnot7 mRNA promotes deadenylation of maternal transcripts during mouse oocyte maturation. *Biol. Reprod.*, **93**, 48.
62. Chang,H.M., Triboulet,R., Thornton,J.E. and Gregory,R.I. (2013) A role for the Perlman syndrome exonuclease Dis3l2 in the Lin28-let-7 pathway. *Nature*, **497**, 244–248.
63. Balagopal,V. and Parker,R. (2009) Polysomes, P bodies and stress granules: states and fates of eukaryotic mRNAs. *Curr. Opin. Cell Biol.*, **21**, 403–408.
64. Eulalio,A., Behm-Ansmant,I. and Izaurralde,E. (2007) P bodies: at the crossroads of post-transcriptional pathways. *Nat. Rev. Mol. Cell Biol.*, **8**, 9–22.
65. Standart,N. and Weil,D. (2018) P-bodies: cytosolic droplets for coordinated mRNA storage. *Trends Genet.*, **34**, 612–626.
66. Mitchell,P., Petfalski,E., Shevchenko,A., Mann,M. and Tollervey,D. (1997) The exosome: a conserved eukaryotic RNA processing complex containing multiple 3′→5′ exoribonucleases. *Cell*, **91**, 457–466.
67. Doamekpor,S.K., Gozdek,A., Kwasnik,A., Kufel,J. and Tong,L. (2020) A novel 5′-hydroxyl dinucleotide hydrolase activity for the DXO/Rai1 family of enzymes. *Nucleic Acids Res.*, **48**, 349–358.
68. Horvathova,I., Voigt,F., Kotrys,A.V., Zhan,Y., Artus-Revel,C.G., Eglinger,J., Stadler,M.B., Giorgetti,L. and Chao,J.A. (2017) The dynamics of mRNA turnover revealed by single-molecule imaging in single cells. *Mol. Cell*, **68**, 615–625.
69. Eulalio,A., Behm-Ansmant,I., Schweizer,D. and Izaurralde,E. (2007) P-body formation is a consequence, not the cause, of RNA-mediated gene silencing. *Mol. Cell. Biol.*, **27**, 3970–3981.
70. Hubstenberger,A., Courel,M., Benard,M., Souquere,S., Ernoult-Lange,M., Chouaib,R., Yi,Z., Morlot,J.B., Munier,A., Fradet,M. *et al.* (2017) P-body purification reveals the condensation of repressed mRNA regulons. *Mol. Cell*, **68**, 144–157.
71. Zhang,B. and Herman,P.K. (2019) It is all about the process(ing): P-body granules and the regulation of signal transduction. *Curr. Genet.*, **66**, 73–77.